NASA TECHNICAL NOTE

NASA TN D-6086

NASA TN D-6086

EXPERIMENTAL RESULTS OF HIGH-CURRENT ARCS DRIVEN SUPERSONICALLY IN STRAIGHT AND CIRCULAR CHANNELS

by Alexander P. Sabol, Roger B. Stewart, and Roy J. Duckett

Langley Research Center
Hampton, Va. 23365

NATIONAL AERONAUTICS AND SPACE ADMINISTRATION • WASHINGTON, D. C. • DECEMBER 1970

1. Report No.	2. Government Accession No.	3. Recipient's Catalog No.
NASA TN D-6086		

4. Title and Subtitle

EXPERIMENTAL RESULTS OF HIGH-CURRENT ARCS DRIVEN SUPERSONICALLY IN STRAIGHT AND CIRCULAR CHANNELS

5. Report Date: December 1970

6. Performing Organization Code:

7. Author(s)

Alexander P. Sabol, Roger B. Stewart, and Roy J. Duckett

8. Performing Organization Report No.: L-6890

9. Performing Organization Name and Address

NASA Langley Research Center
Hampton, Va. 23365

10. Work Unit No.: 129-02-22-06

11. Contract or Grant No.:

12. Sponsoring Agency Name and Address

National Aeronautics and Space Administration
Washington, D.C. 20546

13. Type of Report and Period Covered: Technical Note

14. Sponsoring Agency Code:

15. Supplementary Notes

16. Abstract

Quantitative information concerning the static pressure associated with moving arcs and the arc velocity as a function of the Lorentz force for arc currents as high as 8000 amperes is given for magnetic-field strengths of 0.64 and 1.28 webers/meter^2. With the aid of ultra-high-speed photography and rapid-response pressure gages, results revealed that a single abrupt bow shock ahead of the arc did not occur but that a network of many small primary shocks preceded the luminous zone. In the circular channel tests, different gases and air were used at different densities. These tests, in which the arc ran through its own heated wake, indicated that the arc velocity is faster than that in a straight channel and depends on the gas density to the one-half power for the steady-state condition. During arc start-up periods, the arc velocity is approximately linearly dependent on the applied Lorentz force.

17. Key Words (Suggested by Author(s))

Electric arcs
Supersonic arcs
Straight channels
Circular channels
Unsteady behavior

18. Distribution Statement

Unclassified – Unlimited

19. Security Classif. (of this report)	20. Security Classif. (of this page)	21. No. of Pages	22. Price*
Unclassified	Unclassified	33	$3.00

*For sale by the National Technical Information Service, Springfield, Virginia 22151

EXPERIMENTAL RESULTS OF HIGH-CURRENT ARCS DRIVEN SUPERSONICALLY IN STRAIGHT AND CIRCULAR CHANNELS

By Alexander P. Sabol, Roger B. Stewart,
and Roy J. Duckett
Langley Research Center

SUMMARY

An experimental study has been made to determine the behavior of high-current electric arcs magnetically driven to supersonic velocities relative to the undisturbed medium in straight and circular channels. Quantitative information concerning the static pressure associated with moving arcs and the arc velocity as a function of the Lorentz force for arc currents as high as 8000 amperes is given for magnetic-field strengths of 0.64 and 1.28 webers/meter^2. With the aid of ultra-high-speed photography and rapid-response pressure gages, results revealed that a single abrupt bow shock ahead of the arc did not occur but that a network of many small primary shocks preceded the luminous zone. In the circular channel tests, different gases and air were used at different densities. These tests, in which the arc ran through its own heated wake, indicated that the arc velocity is faster than that in a straight channel and depends on the gas density to the one-half power for the steady-state condition. During arc start-up periods, the arc velocity is approximately linearly dependent on the applied Lorentz force.

INTRODUCTION

The magnetically driven arc is vital to a number of magnetofluidynamic devices, such as pulsed and steady Faraday type accelerators and magnetically rotated arc heaters. In spite of these technical applications, investigations of the fundamentals of the interaction of arcs moving supersonically with respect to the undisturbed surrounding medium have been limited up to the present time. Of the studies made, two different methods of arc observation have been employed. In reference 1, a supersonic stream impinged an arc held between parallel rail electrodes by an electromagnetic force; in reference 2, the arc was magnetically moved through the medium. Both methods allowed the study of different but pertinent aspects of the arc, but with a stationary arc the root conditions of an arc moving over a surface are not simulated. Of particular interest is the shock system

associated with the moving arc. In references 3 and 4, a shock front was found to lead a luminous front. Although such types of phenomena have been studied, the arc-shock phenomenon is not well understood at this time.

The objective of the present investigation was to study the electric arc moving supersonically in straight and circular channels for the purpose of understanding the associated shock mechanism. Efforts were made to identify the source of the shock disturbance as well as the nature of the leading shock wave ahead of the luminous arc region. Data included short duration schlieren photography and measurements of static pressure, arc velocity, arc current, magnetic field, and electric power input. In the circular channel, the rotational velocities of the arc were observed in both open-wall and closed-wall channels. The closed-wall channel permitted tests with different gases and also with air at different densities. An attempt was made to relate these findings to those in reference 2 where arc velocity was found to be affected by preheating the cathode.

SYMBOLS

a	speed of sound, m/sec
B	magnetic field strength, Wb/m^2
C_d	drag coefficient for cylindrical body
C_p	specific heat at constant pressure, $J/kg\text{-}^oK$
d	frontal width of arc, m
E	electric field intensity, V/m
f	friction factor
j	electric current density, A/m^2
J	total electric current, A
m	molecular weight, kg
M	Mach number
p	pressure, N/m^2

p_i initial pressure, N/m^2

R universal gas constant, $J/^oK$-(kg mole)

T temperature, ^oK

u gas velocity relative to arc, m/sec

u_{abs} absolute velocity of conducting species, m/sec

v arc velocity, m/sec

x distance within discharge zone

γ adiabatic index

ρ gas density, kg/m^3

σ electrical conductivity, mhos/m

Subscript:

i condition at forwardmost point in arc discharge zone

APPARATUS

Figure 1(a) shows the apparatus used in the arc study. (This photographic view is parallel to the direction of the magnet flux lines.) The device consisted of two different arc discharge channels electrically connected in series and placed in the core of two large magnetic coils. A circular arc channel with a fixed outer diameter was located within the confines of a horseshoe-shaped arc channel (fig. 1(b)). The outer electrode of both channels operated at a negative potential. Two high-current arcs (up to 8000 A) were simultaneously created, one in each channel, by a rapidly operated sparking device at point A and by a thin shorting wire tab at point B. In the presence of magnetic-field strengths of 0.64 and 1.28 Wb/m^2, both arcs moved in a clockwise direction. The length of the horseshoe-shaped arc channel was 2.3 times that of the circular arc channel. The action of the magnetic field extinguished the arc in the horseshoe-shaped channel at point C and caused the other arc to die also. Thus, the arc in the horseshoe channel became the control or rapidly operating high-current switch for the arc in the circular channel. In an effort to minimize the contamination of the medium by vaporized metal, a thin wire

tab completed the electrical circuit at point B. This wire tab was 0.0254 cm in diameter and 1.27 cm long. The electrical discharge then vaporized 0.0057 g of metal amounting to 3.5 percent of the weight of air contained within the circular electrodes. The core of two large magnetic coils contained both electrode channels. These coils had an outside diameter of 1.3 m and a working core diameter of 58 cm. The uniformity of the magnetic field was better than 1.0 percent over the entire core area. The coils and the arc were separately energized by 10-MW silicon rectifier dc power supplies. The magnetic field remained constant during the lifetime of the arc. The ripple in the coil current amounted to ± 0.5 percent and had a constant peak-to-peak frequency of 720 Hz.

The arc gap or electrode separation in both the open-wall and closed-wall circular channels was 1.27 cm and the width of both channels was 2.54 cm. Electrode material for all tests was type 347 stainless steel. For some tests, in order not to hinder photographic studies windows of clear acrylic plastic were applied to the circular channel to obtain data showing the effects of closed-wall-channel operation, to permit the use of different gases, and to maintain a desired initial pressure. Oscillographs recorded both the arc current and arc voltage. (See appendix A.) By use of photomultiplier tubes which detected the light from the moving arc at two separated stations, arc velocities could be determined from resulting oscilloscope traces by noting the time of flight. Measurements show the pressure disturbance in the vicinity of the moving arc. In the closed-wall channel tests, the monitoring device sensed the pressure through a hole in the side wall; in the open-wall-channel tests, the pressure transducer was simply located in the approximate but not the same position as in the closed channel tests, which was 1.59 cm from the center line of the arc channel. Oscilloscopes monitored the arc pressure disturbance by means of a nonmagnetic piezoelectric pressure transducer. A strong and steady or a slowly varying magnetic field had no effect on this gage, but a strong current pulse in the immediate vicinity of the gage might have had an effect on it. The gage and amplifier system had an approximately 5-μsec rise time.

Photographs of the arcs were taken with a double-frame image-converter camera incorporating a beam splitter which allowed both frames to view the image from the same angle. An electrical circuit permitted taking two time-displaced photographs. The object viewing time varied from 100 to 1000 nsec. This camera also permitted the use of schlieren optics to observe the pressure disturbances created about the arc. Observations of the arc in the circular channel were made in region I and those in the straight channel, in region II. (See fig. 1(b).)

ARC STRUCTURE

The arc was observed in both the straight channel and in the circular channel. The observation areas are indicated in figure 1(b). Straight channel tests were made with the

open-wall channel only and during the time the arc was passing through an otherwise undisturbed atmosphere. The arc was observed in both the open-wall and closed-wall channels of the circular channel during the period of the first arc pass and during repeated arc passes. As a result of the arc passing through its own heated wake, the rotational speed increased and, in some instances, up to 15 rotations were observed for a single pass of the control arc.

The arc current had a ripple of ± 2.7 percent at a constant frequency of 720 Hz. This ripple was measured by placing an 0.0079-Ω resistor in the circuit as a dummy load. The current rise time through this resistor was 0.45 msec which was shorter than the total arc duration of 4 to 5 msec. However, in tests the time to reach this maximum current was sometimes altered by the presence of the moving arcs.

Straight Channel Tests

The study of the motion of the arc column in the straight channel at a 1.27-cm gap setting made use of high-speed photography. For these tests, both ordinary photographs and schlieren photographs were taken. Photographs of the moving arc taken at two different but closely spaced time intervals showed an apparent erratic forward movement of the arc. Two such high-speed photographs of the same arc taken 20 μsec apart (fig. 2) reveal the severity of the arc column distortion resulting from the erratic arc motion. Although the average arc column velocity was 370 m/sec during the period of observation, the upper portion of the column had a higher local velocity of 412 m/sec. Such erratic behavior of portions of the arc column was typical of the arc progressions, and severe arc column distortions have also been observed by other investigators (ref. 5).

This erratic motion produced scatter in the measurements of the arc velocity. The effect on the flow is evident in figure 3. The erratic forward motion with some portions of the arc moving faster than the others resulted in a different type of flow field from the single steady shock ahead of a solid body. The photographs revealed that multiples of small shocks or shock wavelets existed in front of the arc. The unsteady forward motion of the arc and the intermittent local expansion of the air affected by the electrical discharge apparently produced these wavelets. The wavelets ballooned or expanded at speeds greater than the average arc velocity. A continuous process was thus established by the supersonically moving arc which created a shock-filled zone immediately preceding the arc (fig. 3(a)). As seen in figures 3(b) and (c), this shock zone ahead of the arc decreased in depth as the average arc speed increased. As measured from the leading shock to an arbitrary point associated with the arc, figure 4 quantitatively shows the variation of shock zone depth with arc velocity. At low velocities, the primary shock zone extended in excess of 3.5 cm. Such behavior of the leading shock standoff distance is also characteristic of supersonic solid body motion.

The rapid-response pressure transducer verified and gave more information of this leading shock zone. In the open channel tests, this device was placed in a position to respond only to lateral pressure disturbances. However, because of its particular location away from the center of the arc path, the pressure transducer did not sense the true static pressure of the arc. Also, due to the particular orientation of the face of this sensing element, the total aerodynamic arc pressure was not measured. This pressure would have been much higher than the observed static pressures as can be determined by comparing with pressures presented in reference 2. The pressure disturbances were recorded on oscillograms such as that shown in figure 5(a). Because of the rapid (μsec) response time of the pressure instrument, the random local plasma fluctuations within the arc apparently caused the ragged appearance of the traces.

The arc speed and arc width were determined from the oscillograph trace of the photomultiplier tube outputs. Depending on the sensitivity setting, the tube circuitry generates two types of signals, one from each tube. A setting for low sensitivity produced a small narrow pulse and a high setting produced a broad pulse on the oscillogram. Both types of signals are illustrated in figure 5(a). The record from the high sensitivity setting showed the approximate lighted width of the arc. In addition, the spread of the two pulses indicated the time of flight of the arc between two separated stations from which the arc velocity was obtained. However, during these velocity measurements the exact position of the arc within the broad trace could not be accurately determined. Thus, some error was introduced by a high sensitivity setting. Further, the high setting caused the photomultiplier tube to be sensitive to minor secondary illuminations as would arise from glowing particles or a weak stray discharge. Such a second signal is shown in figure 5(a).

Because of the different axial locations of the light and pressure sensors near the electrodes, the disturbances on the two oscilloscope traces were not coincident with each other (fig. 5(a)). By correcting for this displacement, matching of the two traces showed the correspondence between the pressure history and the history of the luminosity. A sketch showing the resulting deduced location of the shock zone relative to the approximate arc column depth is given in figure 5(b). This location of the primary shock zone coincides with that found in the schlieren photographs of figure 3. The pressure rise in the primary shock zone differs from that expected ahead of a solid moving body where a pressure rise occurs through a single shock wave. In figure 5(b), the pressure rose rapidly ahead of the arc in an almost linear manner from ambient pressure to a maximum value before the onset of luminosity from the arc discharge. The rate of pressure rise in the primary shock zone is not indicative of shock pressure traces generated by a solid body. However, the rate of the pressure rise could be altered by the release of thermal energy alone or in conjunction with a porous body.

As shown in figure 5(b), the pressure disturbance generated by the impulsive motion of the arc reached a maximum at the leading edge of the electrical discharge and then decreased through the arc discharge. A one-dimensional analysis where the arc column is treated as a porous body, in preference to solid-body hypotheses as given by others, indicates that the pressure also decreases through the discharge zone. Thus, the results of this analysis are in qualitative agreement with the experimental results. Appendix B gives the details of this analysis and the results for a hypothetical case.

Circular Channel Tests

The arc was observed in the circular channel both during the first pass where the ambient air was undisturbed by any previous presence of the arc (this was an arc acceleration period) and when the arc had reached an average maximum rotational speed. The circular arc gap was 1.27 cm. For the purpose of noting the effect of gas density on arc velocity, the arc was observed with and without side walls added to the circular channel.

Figure 6(a) is a photograph taken with the image-converter camera of the appearance of an arc in the circular channel at atmospheric pressure with no confining side walls. In this photograph, the electrodes were illuminated by auxiliary lighting to make them visible. The photograph shows the arc during the first pass. As in the straight open channel, the moving arc in the open-wall circular channel assumed a constricted appearance which can be attributed in part to a large degree of cooling. However, in contrast to the appearance observed in the straight channel, the circular channel arc column moves tilted with respect to the radius of the electrode curvature so that the outermost arc portions were swept back. This configuration has been investigated by others (see, for example, ref. 6). Thus, the net magnetohydrodynamic force in the column is directed in part against the outer electrodes.

When transparent side walls were added to the circular channel, the arc appearance changed. The side walls contained a pressure bleed hole to insure that the ambient conditions of the arc remained at atmospheric pressure. As shown in figure 6(b) which is a photograph of the arc in nearly the same location as in figure 6(a), the side walls caused the arc to disperse or broaden along the axis of the channel so that the arc in the closed-wall channel appeared broader than the arc in the open-wall channel. The diffused appearance of the arc is attributed to less cooling offered by the side walls.

Figure 7(a) is a schlieren photograph showing typical disturbances about the arc in the open-wall circular channel. Because of unwanted lingering disturbances which remain in the circular channel, the photograph was taken during the arc start-up period. The phenomenon resembles that for the low-velocity straight rail where weak disturbances lead the arc (fig. 7(b)). Pressure gage measurements show these weak disturbances to be a phenomenon separate from that occurring in the immediate vicinity of the arc as

found in figure 5. Yet the characteristics of the local arc pressure rise appeared to be the same as those of the pressure rise about an arc in the straight open channel except for a much smaller magnitude of peak pressure. The tilt of the arc by the circular channel is an apparent cause for both the reduced pressure and the escape of leading weak disturbances.

A schlieren photograph of and the pressure history and light output from an arc in a circular channel closed by side walls are presented in figure 8. As in figure 6(b), which depicts the light broadening of an arc during the first pass in the closed channel, figure 8(b) shows not only similar weak density variations in the vicinity of the arc but also the same wide distribution of the leading disturbances as found in figure 7(b). In figure 8(a) the low-intensity light from the diffused arc was washed out by the schlieren light source. The pressure measurements in figure 8(b) verify the presence of the observed weak disturbances leading the arc and also show that the measured local arc pressure rise was greatly attenuated. Thus, by photographing the arc during an initial pass in the closed-wall circular channel, the predominant effect noted was that a diffusion took place in both the arc column light output and the primary shock zone disturbance. The resulting pressure rise could not be identified as could the pressure rise in the open-wall channel. Direct comparisons of the observed pressures in the open-wall channel and closed-wall channel could not be made because the pressure transducer could not be placed equally close to the arc in the two tests.

VELOCITY MEASUREMENTS

Open Channel Tests

Arc speeds were measured for a wide range of conditions in both the circular and straight channels in the regions shown in figure 1(b). Velocity measurements were obtained in the circular channel after the arc made several rotations and attained nearly a constant speed. Sample velocities obtained from oscillogram traces such as those in figure 5 are presented in figure 9 for the straight and circular open channels. The velocities are plotted as a function of the applied Lorentz, or driving, force per unit length of arc. This display is compatible with treating the arc column as though it were a solid body (see, for example, ref. 2). The solid body assumption is in contrast with the earlier treatment of the arc column as a porous body. Solid body behavior is given by the following formula:

$$v = \left(\frac{2JB}{\rho d C_d}\right)^{1/2}$$

where JB is the applied electromagnetic force and C_d is a representative drag coefficient. (Since the arc column is assumed to behave as a solid cylindrical body, the drag

coefficient C_d is approximately 1.1.) This expression gives a parabolic relationship between the velocity and the driving force. Two such curves were plotted in figure 9, each for a different value of the arc diameter d. For comparison with previous tests, the best fit straight line from reference 2, showing the average of results obtained in a straight open channel, was also added to the figure. The large scatter of the present tests is attributed to the erratic procession of the arc evidenced in sequence photographs.

In the low power range which is within the transonic and low supersonic regions, the velocities observed for the straight and circular electrodes are approximately the same with the circular channel results only slightly greater in value. Throughout the higher power tests, the arc velocities measured in the circular channel noticeably exceeded those in the straight channel. Two possible causes are advanced: (1) in the circular channel, the arc velocity was measured after several rotations and after the arc passed through its own previously heated wake (thus, the arc passed through a better conducting media); and (2) the ambient air in the arc track assumed a rotational speed in the direction of arc travel which reduced the relative speed of the arc and the surrounding air with a resulting decrease in drag.

In figure 9 a comparison of the test results and the solid body analogy is made. The circular-channel results do not coincide with those of the straight channel. The difference can be analytically accounted for by arbitrarily assuming arc diameters of 2.22 and 0.52 cm. However, because the arc currents in both the straight- and circular-channel tests are identical for the same driving force, the actual arc diameters probably did not appreciably change. Thus, at these high current levels, the solid body analogy may not properly account for drag effects. This analogy does, however, indicate the trend in velocity for both channels at high input currents. However, for these data, the trend could also be considered approximately linear. In the straight channel, the velocity increase is small for a comparatively large current input or, equally, there is a low arc driving efficiency. In contrast, in the circular channel, arc speeds increase approximately twice as fast for the same current input.

Heating and rotational swirl effects on the arc velocity were noted during the short transient conditions of arc start-up. Figure 10 shows the increase in arc velocity with increase in the total applied Lorentz force per unit length for a single arc. An approximately linear increase in arc speed occurs during the start-up period rather than the usual $(JB)^{1/2}$ for the steady-state conditions. During this transient period, both the increase in local ambient gas temperature and the increase in rotational gas motion in the same direction as the arc were apparent causes of the faster rise in arc speed with current increase.

Density Effects

Density effects on arc velocity were determined by using several gases and by controlling the ambient gas density. Air, helium, and argon were used as the ambient fluid. All tests to explore density effects were made with side walls added to the circular channel. Several tests incorporated a pressure bleed hole in the side walls to keep the confined gas at atmospheric pressure. Without the pressure bleed, the ambient gas remained at approximately constant density during the test. Figure 11 shows the arc velocity as a function of the gas molecular weight obtained at atmospheric pressure. These results are compared with predictions obtained by using the solid body analogy. Tests were made at conditions where all parameters could be considered approximately constant, that is, at a fixed value of applied current and magnetic field. From

$$JB = \frac{1}{2} \rho d C_d v^2$$

and

$$\frac{p}{\rho} = \frac{RT}{m}$$

is obtained

$$v = \left(\frac{2JBRT}{dpC_d m} \right)^{1/2}$$

Thus, at a constant Lorentz force and when T, p, C_d, J, and d are assumed constant,

$$v \propto \frac{1}{\sqrt{m}}$$

Although the parameters considered constant might vary from one gas to another, general agreement exists between experiment and theory (fig. 11). This agreement suggests that the arc velocity is a parabolic function of the density. Experiments were then extended to tests in the same gas at different densities. In these tests the volume remained constant for the circular channel and the initial gas pressure was regulated. Thus, the average density remained approximately independent of the gas temperature rise. As in the foregoing derivation, theory predicts

$$v \propto \frac{1}{\sqrt{p}}$$

The data obtained from this relationship are compared with experimental data in air in figure 12. Figure 11 shows the same trend in velocity. In both figures, the arc velocity varied approximately as the square root of the average gas density. Test results reported in reference 2 indicated that higher arc velocities could be obtained by heating the cathode. In the present tests, the effect of the gas density on arc velocity may help to explain in

part the results in reference 2. In that study, the arc was able to move faster possibly because of the hotter, lower density air next to the heated electrode.

SUMMARY OF RESULTS

Experimental results obtained for high-current electric arcs at atmospheric pressures which were magnetically driven to supersonic velocities in 1.27-cm straight and circular arc channels indicated that

1. In both straight and circular open channels, an electric arc progresses in an erratic manner so that portions of the arc sporadically advance above the average speed of the main arc column.

2. In the straight and open channel, such erratic motion continually gives rise to disturbances which produce a pressure history in front of the arc different from that of the usual pressure rise ahead of a supersonically moving solid cylindrical body (this was obtained from schlieren studies and pressure measurements about the arc). These disturbances cause a primary pressure rise to occur over a broader region when compared with that in a bow shock about a solid cylindrical body of approximately the same diameter as the luminous arc and at comparable velocities.

3. In the straight and open channel, the width of this primary shock region is affected by the arc velocity so that at higher observed arc velocities it was narrow and more closely resembled the condition about a solid body. At the lower velocities, measurements showed this primary shock zone to extend in excess of 3.5 cm.

4. The rise in pressure ahead of the arc was followed by a decrease in pressure (this was inferred by static-pressure measurements made in the vicinity of the arc path). The observation of a decrease in pressure compares qualitatively with a theoretical conclusion concerning the fall in pressure through an arc discharge. The theory is based on simplifying assumptions treating the arc as a porous body.

5. The arc velocity in the circular channel is a function of the inverse square root of the prevailing gas density. Tests made in gases of different densities as influenced by the molecular weight showed this to be true as did tests in closed-wall channels where the density of air was controlled by the initial gas pressure.

6. In the circular channel, the arc velocity varies approximately linearly with the applied Lorentz force JB during the transient period of arc start-up rather than with $(JB)^{1/2}$.

Langley Research Center,
National Aeronautics and Space Administration,
Hampton, Va., September 28, 1970.

APPENDIX A

DESCRIPTION OF INSTRUMENTATION

Velocity Measurements

A schematic diagram of the apparatus for making the velocity measurements is shown in figure 13. The collimating holes lay perpendicular to the path of the arc. The light from the arc passed through the holes and was transferred to the photomultiplier tubes by means of light pipes. A transistorized emitter follower matched the high output impedance of each photomultiplier tube to the impedance of the coaxial cable connecting the output of the photomultiplier to the input of the dual beam oscilloscope.

The following method was used to measure the arc velocity. The output signal of an upstream emitter follower triggered the oscilloscope. The oscilloscope operated in a delayed sweep mode which allowed the sweep time of the measuring circuit to function on a short time scale and, thus, the accuracy of the measurement was increased. One photomultiplier was located at a precisely measured location upstream from a second photomultiplier so that the traces on the oscilloscope indicated a time displacement of the arc luminosity. This time difference and the distance between the collimating holes determined the arc velocity. The velocity in the circular rails was calculated by the foregoing procedure as well as by the following procedure. The time scale was increased so that the arc would make more than one revolution around the circular electrodes. The velocity was calculated by using the total circular distance and the time for the arc to return to its initial position. The increase in arc velocity due to passing through its own previously heated wake is illustrated by observing the difference in time from the first pass to the second pass, and so forth.

The camera photographed the traces on the oscilloscope by preopening the shutters which allowed the traces to be automatically produced by the trigger circuits. The shutters then closed and the grid scales were superimposed for measurement purposes. Some typical traces are shown in figure 14.

The accuracy of the photoelectric technique depends upon the determination of the time separation of the luminous region of the arc column and of the separation distance between collimating holes. The hole separation distance can be determined very accurately. The major source of error in this measurement is the determination of the time differences. Since each measurement represents essentially a unique event, no attempt was made to obtain a statistical analysis of the data. However, it is reasonable to say that the data are accurate to within a few percent. The significance of the preceding statement is that the scatter in the data in figure 9 represents true variations in arc velocity and not a measurement error.

APPENDIX A

Arc Voltage and Current Measurements

Figure 15 shows a schematic diagram of the apparatus for making the voltage and current measurements. All measurements came from oscilloscope displays of the voltages and from photographs of the resultant wave forms. This technique allowed the time history of the voltage and current to be obtained. Although the applied magnetic field was held constant during the measurement, extreme care was necessary in positioning the leads to the voltage measuring circuits to reduce the induced magnetic-field effects produced by the short-duration arc. Each voltage from the arc passed through coaxial cables and was imposed across a voltage divider consisting of ten 10 000-Ω noninductive resistors. The voltage from the last resistor was then coupled to the oscilloscope by means of an additional coaxial cable. This system was checked for response by applying a known square wave signal to the input terminal and measuring the output signal on the oscilloscope. The results of these tests indicated that the response of the system was at most one-tenth of any signal measured in the tests. The current was obtained by measuring the voltage drop across a water-cooled stainless-steel resistor having a measured resistance of 0.00791 Ω.

Pressure Measurements

A quartz crystal pressure transducer detected the transient pressures associated with the arc. The signal from this gage energized a capacitive feedback charge amplifier and the output was then displayed as an oscilloscope trace. Figure 16 shows the gage arrangement. Both the gage and mounting block were made of nonmagnetic stainless steel and the transmission cable was housed in additional webbed sheathing to reduce any transient disturbances. The location of the charge amplifier allowed the low noise transmission cable from the gage to pass along magnetic flux lines of the applied field rather than across these lines. The gage rise time was 1 μsec and the rise time of the rest of the system including transmission line, charge amplifier, coaxial cable, and oscilloscope was estimated to be not in excess of 4 μsec. Numerous calibrations of the gage and amplifier system verified the original factory calibration factors. A thin ablative coating of rubber adhesive was placed on the nose of the quartz transducer to protect the surface from high-temperature gases from the arc. Figure 14 shows the system response due to multiple passes of the arc in a circular electrode.

Schlieren and Photographic System

Of particular interest to this study was the flow field about an arc moving at supersonic speeds. A single-pass parallel-light schlieren system was used for this purpose (fig. 17). The light from a short-duration (approximately 1.0 sec) spark light source was collimated by a 2.4-m-focal-length first-surface parabolic mirror and passed through the

disturbance about the arc. The schlieren effect was achieved by a reflecting knife edge at the focal point of each mirror. A pulse generated by a circuit built into the image-converter camera triggered the spark light source. The controlling signal for this circuit and for the camera was created by the main arc current at the moment of arc breakdown.

Conventional pictures made by removing the knife edge near the camera provided a direct view of the arc. The spark light source was also inactivated. The double-frame image-converter camera contained a beam splitter to permit either frame to view the object from the same angle and an electrical circuit to permit taking two time displaced photographs. The viewing time varied from 100 to 1000 nsec. Photographs of the arcs were made in either the circular channel or straight channel shown in figure 1.

APPENDIX B

ANALYTICAL DETERMINATION OF PRESSURE VARIATION IN ARC

In order to examine the phenomenon inside the arc discharge, a porous model for the arc is used. This assumption is in contrast to studying the phenomenon outside the arc by using a solid-body theory. The model of the moving arc used for the theoretical analysis is shown in figure 18. Illustrated is a straight channel bounded at the top and bottom by two electrodes. The electrode polarity causes the discharge to move from right to left. The frontal area of the discharge is considered unity and the observer is assumed to move with the phenomenon. Thus, in the figure the flow moves from left to right and passes through both the primary shock and discharge zones. For this analysis several simplifying assumptions were made: (1) the arc is porous and remains erect to the direction of motion, (2) the conductivity is a scalar quantity, (3) the flow field and magnetic field are uncoupled, and (4) electrode losses are neglected as well as the viscous, heat conduction, and radiation losses. The phenomenon in the arc column can then be described by the following relationships:

Continuity

$$\frac{d\rho}{\rho} + \frac{du}{u} = 0$$

Momentum

$$dp + \rho u\, du = jB\, dx - f$$

Energy

$$\rho C_p\, dT + \rho u\, du = jB\, dx + \frac{j^2}{\sigma u}\, dx$$

Velocity of sound plus equation of state

$$C_p\, dT = \frac{a}{\gamma - 1}\left(\frac{dp}{p} - \frac{d\rho}{\rho}\right)$$

Ohm's law

$$j = \sigma\left(E - u_{abs}B\right)$$

In the foregoing equations, a and T are the local speed of sound and local temperature within the arc column or discharge zone (fig. 18). In Ohm's law, because the current density j is within the moving discharge and the external magnetic field is stationary, the absolute flow velocity u_{abs} must be used.

In using these equations to describe the arc characteristics, they are first transformed into the usual differential form. The solution for a particular set of conditions is

then obtained by a numerical integration method. However, to avoid trivial solutions due to the absence of friction losses and to obtain meaningful solutions, a friction factor f accounting for friction losses was added to the momentum equation. By using this friction factor, the differential form of the equations becomes

$$\frac{du}{u} = \frac{M^2}{1 - M^2}\left(jB + \frac{\gamma - 1}{\sigma u} j^2 \frac{dx}{\rho u^2} - f \frac{u_{abs}}{u} dx\right)$$

$$\frac{dM}{M} = \frac{M^2(\gamma + 1)}{2(1 - M^2)}\left(jB + \frac{\gamma - 1}{\gamma + 1} \frac{1 + \gamma M^2}{u} j^2\right)\frac{dx}{\rho u^2} - f \frac{u_{abs}}{u}\left(1 + \frac{\gamma - 1}{2} M^2 dx\right)$$

$$\frac{dp}{p} = - \frac{\gamma M^2}{1 - M^2}\left[jB + (\gamma - 1)M^2 j^2\right]\frac{dx}{\rho u^2} + f \frac{u_{abs}}{u}\left[1 + (\gamma - 1)M^2 dx\right]$$

$$\frac{dT}{T} = - \frac{\gamma - 1}{1 - M^2} M^2\left(jB - \frac{\gamma - 1}{u} M^2 j^2\right)\frac{dx}{\rho u^2} + f \frac{u_{abs}}{u}(\gamma - 1)M^2 dx$$

Because of the complexity of these equations, finding a solution was facilitated by use of a computing machine. In the process, a value for f was preselected and then the values on the right-hand side were considered constant only over an incremental distance dx. The calculated values are then used to obtain solutions over the next finite step, and so on. The calculations stopped at $M = 1$. This limitation corresponds to that given by detonation theory. Basically, energy added to flow which leaves the discharge zone faster than the speed of sound cannot be transmitted forward through the zone as a pressure wave to support the primary shock zone.

The results of one sample calculation are shown in figure 19. They are presented only to show the calculated trend of the pressure and of other parameters through the arc zone and cannot be quantitatively applied to the present tests because of the absence of certain needed measurements. However, the results qualitatively agree with the observations of actual tests.

REFERENCES

1. Bond, Charles E.: Slanting of a Magnetically Stabilized Electric Arc in Transverse Supersonic Flow. Phys. Fluids, vol. 9, no. 4, Apr. 1966, pp. 705-710.

2. Sabol, Alexander P.; Stewart, Roger B.; and Duckett, Roy J.: An Experimental Study of the Behavior of High-Current Arcs Driven by Strong External Magnetic Fields. NASA presented at Eighth Symposium on Engineering Aspects of Magnetohydrodynamics (Stanford Univ.), Mar. 28-30, 1967.

3. Jeanmaire, Peter: Visualization of the Shock Front in an Electromagnetic Shock Tube. Phys. Fluids, vol. 6, no. 7, July 1963, pp. 1028-1029.

4. Brinkschulte, H.; and Muntenbruch, H.: Interferometrische Untersuchungen an elektromagnetisch beschleunigten Stosswellen. Z. Naturforsch., Bd. 20a, Heft 2, Feb. 1965, pp. 196-202.

5. Dethlefsen, Rolf; and Roman, Ward C.: Electric Arc Attachment, Heat Transfer, and Electrode Erosion of High Current Arcs Driven Magnetically Over Metal Electrodes. Ninth Symposium on Engineering Aspects of Magnetohydrodynamics, Space Inst., Univ. of Tennessee, 1968, pp. 17-18.

6. Adams, V. W.: The Influence of Gas Streams and Magnetic Fields on Electric Discharges. Pt. 2: The Shape of an Arc Rotating Round an Annular Gap. Tech. Note No. Aero 2915, Brit. R.A.E., Sept. 1963.

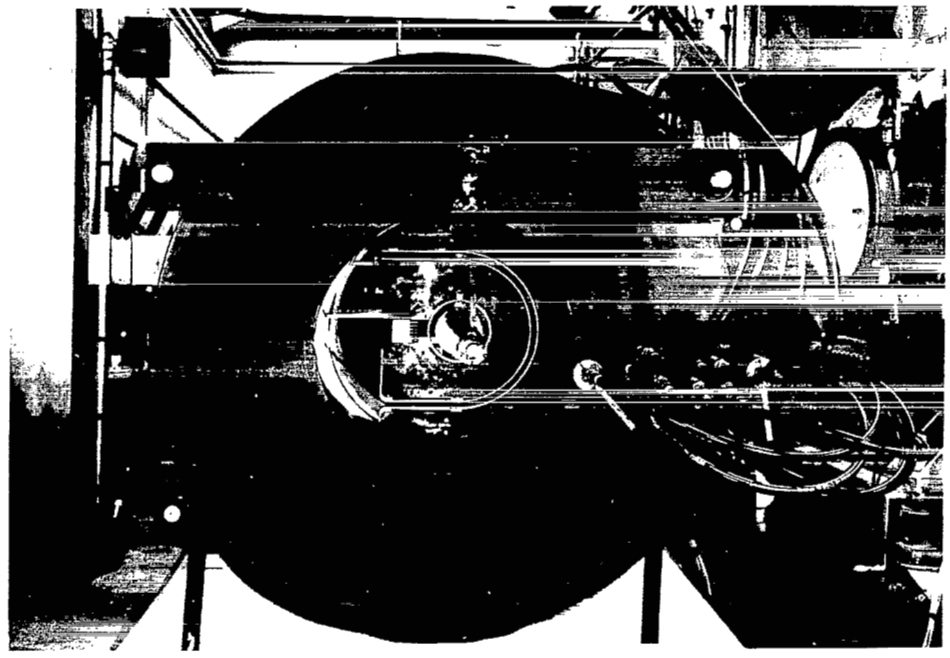

L-68-1418

(a) Circular and horseshoe-shaped arc channels.

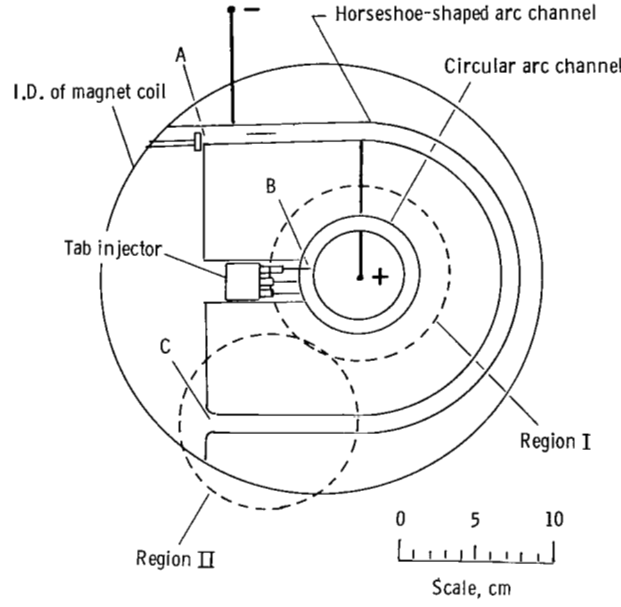

(b) Arc channel components.

Figure 1.- Arc channels within core of two magnet coils.
Coil outside diameter, 1.3 m; inside diameter, 0.58 m.

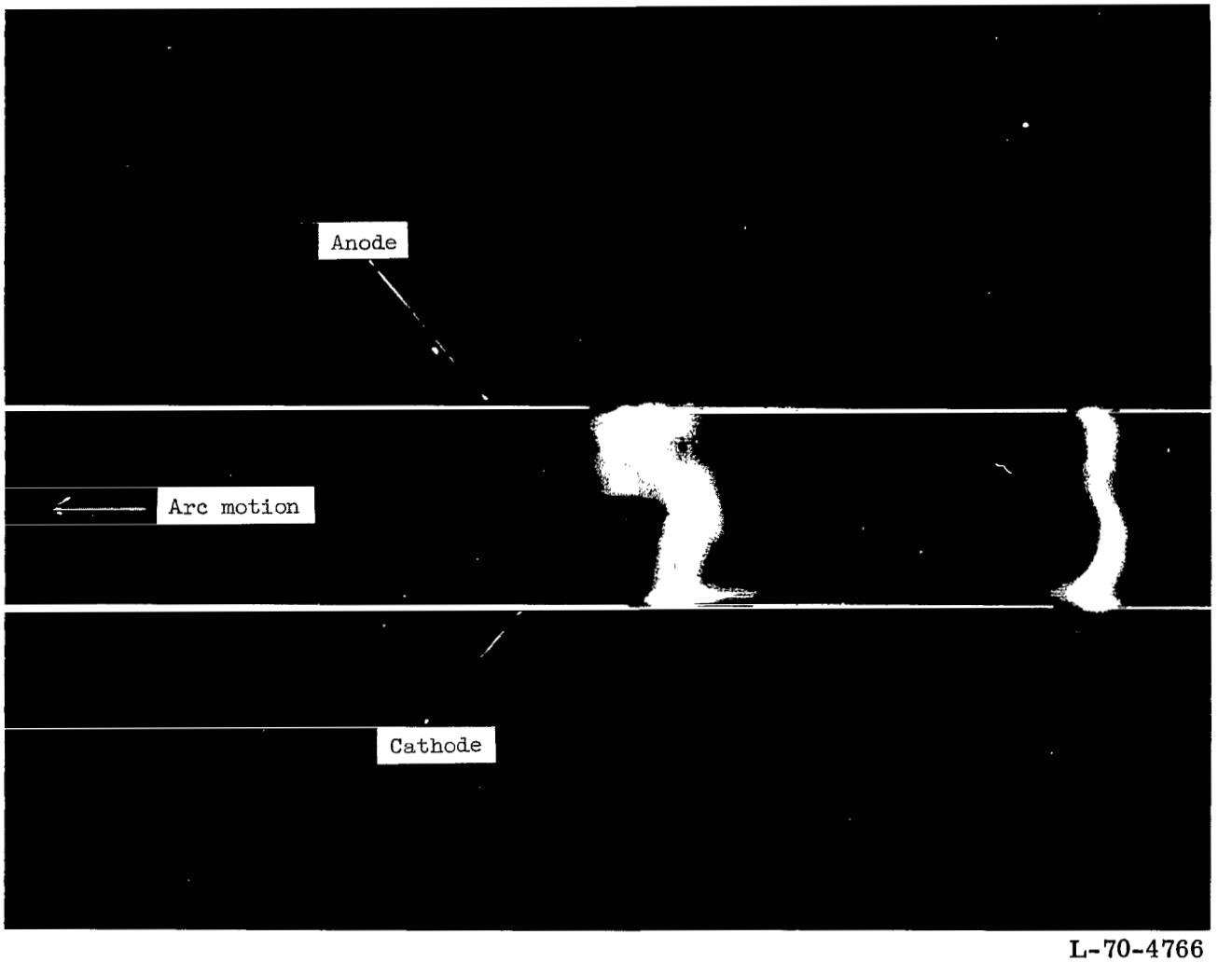

L-70-4766

Figure 2.- Two photographs joined to show a typical variation in same arc column posture during a 20-μsec period. Average arc velocity, 370 m/sec; exposure time, 100 nsec.

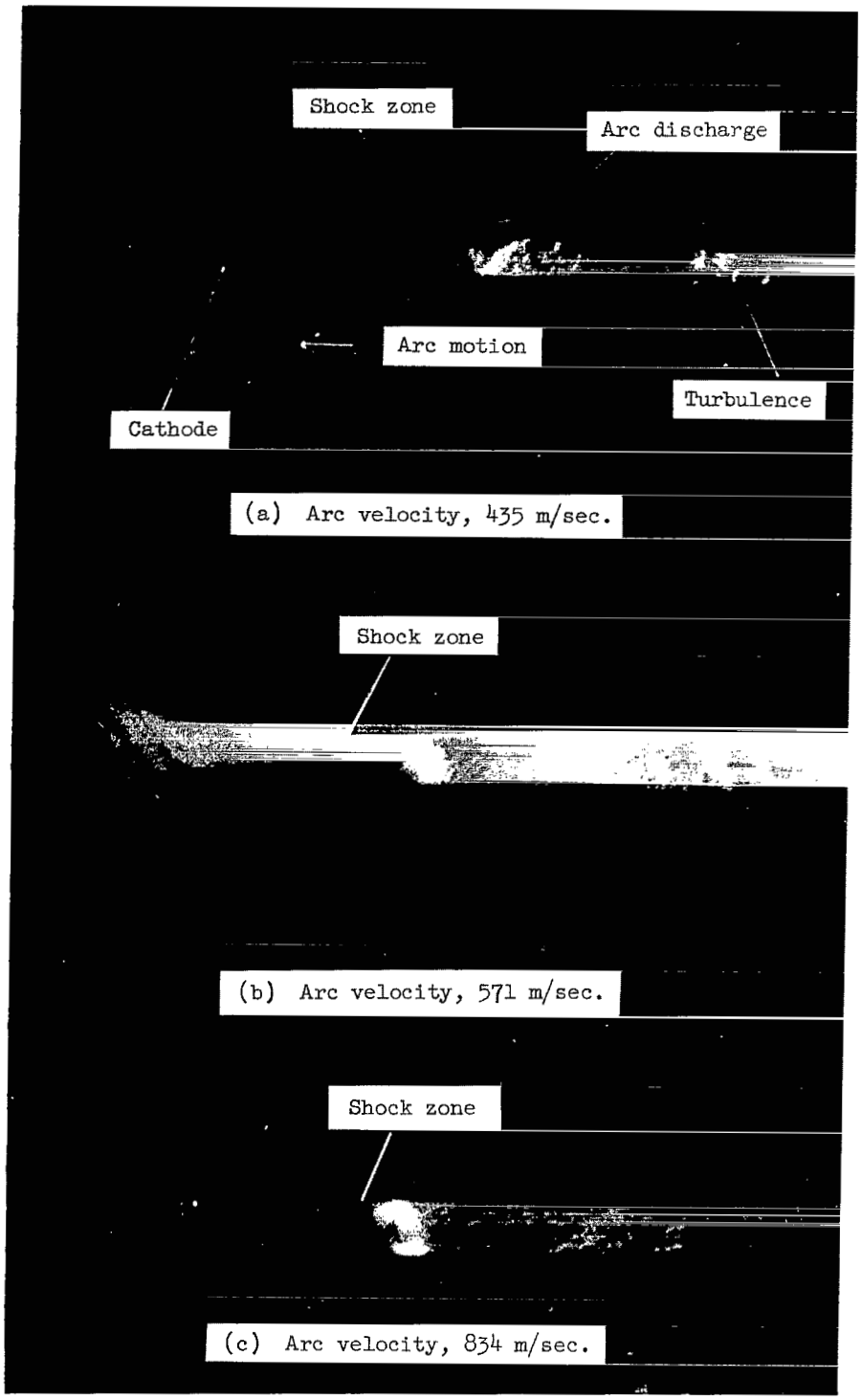

L-70-4767

Figure 3.- Schlieren photographs showing the appearance of local shocks and of the leading shock zone produced by jerking forward motions of the arc.

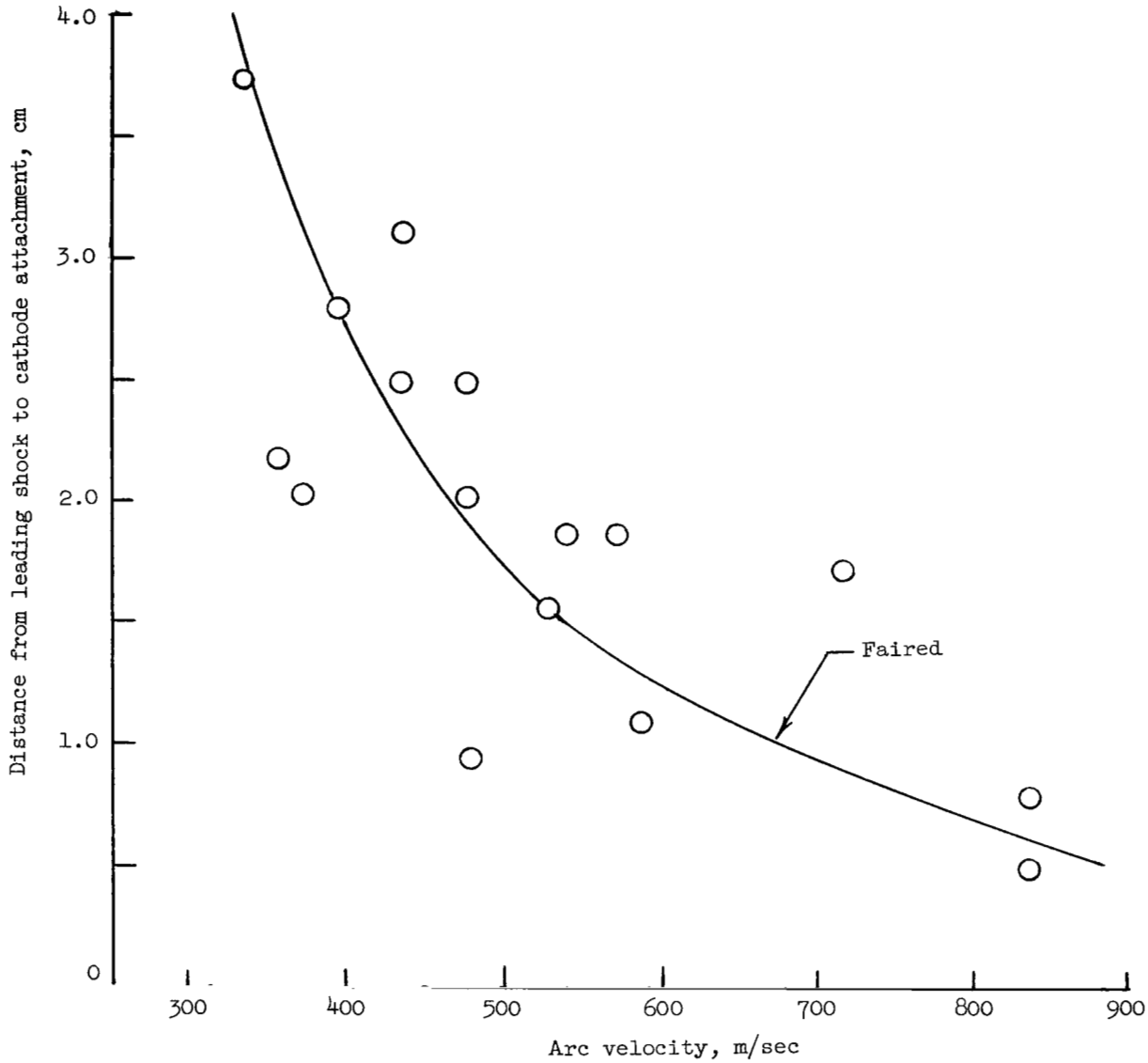

Figure 4.- Variation in shock region depth preceding arc.

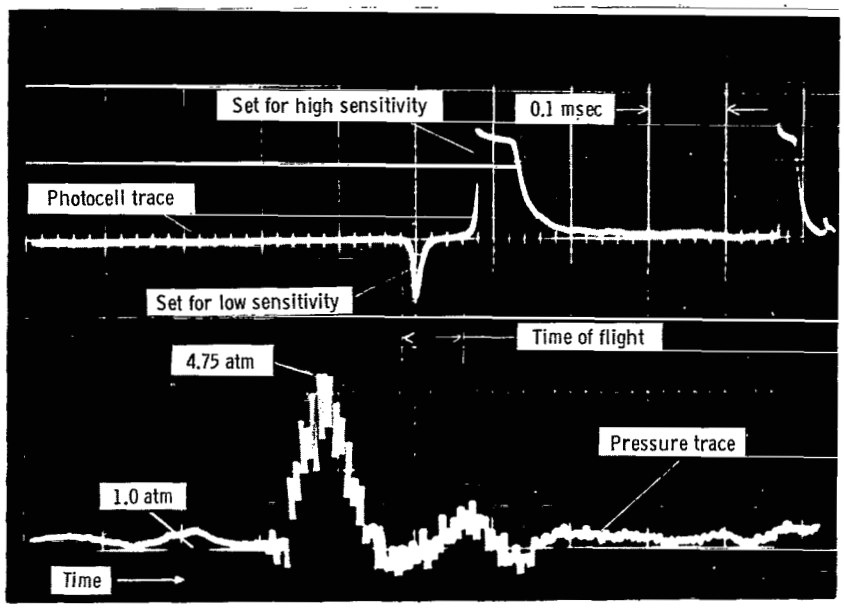

L-70-4768

(a) Oscilloscope traces of pressure and photomultiplier tube outputs from an arc in a straight open channel. (1 atm = 101 325 N/m^2.)

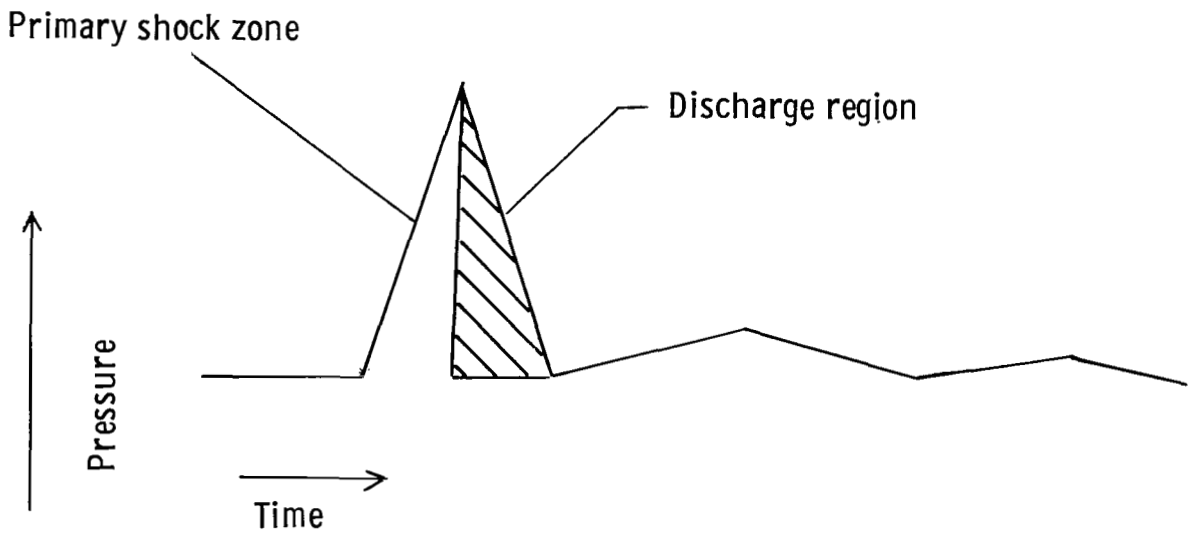

(b) Occurrence of static pressure when corrected for light and pressure sensor displacement.

Figure 5.- Position of arc relative to static-pressure history. Arc velocity, 713 m/sec.

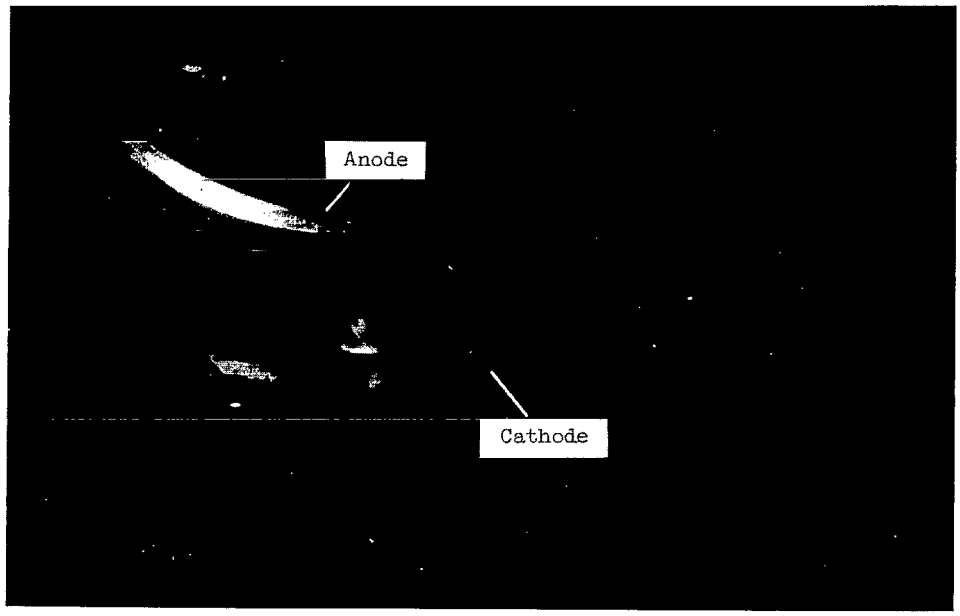

(a) Open-wall channel; arc velocity, 364 m/sec.

L-70-4769

(b) Closed-wall channel; arc velocity, 435 m/sec.

Figure 6.- Arcs in circular channels.

L-70-4770

(a) Schlieren photograph.

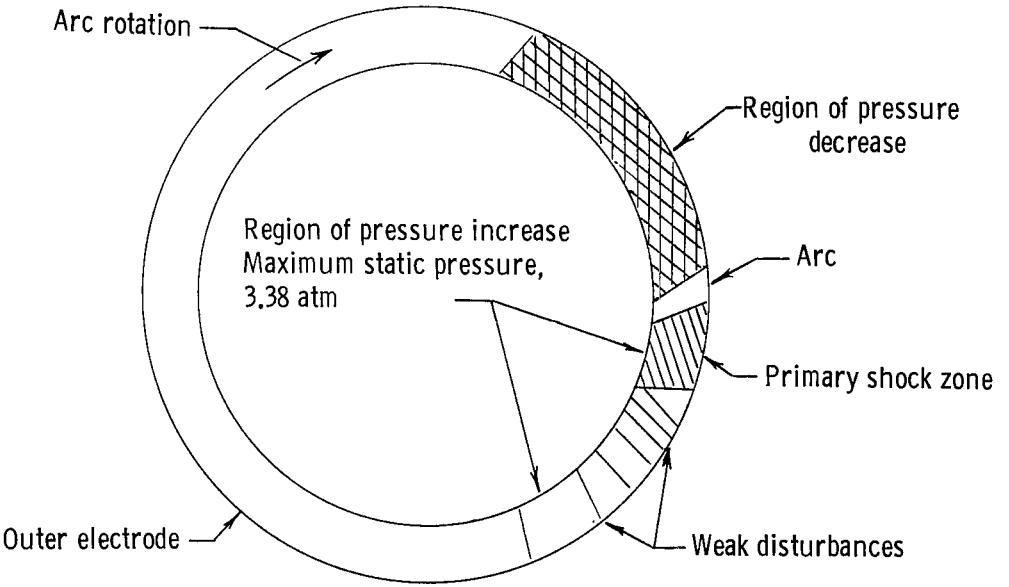

(b) Details of phenomenon.

Figure 7.- Pressure disturbances about an arc in an open-wall circular channel. Arc velocity, 1089 m/sec.

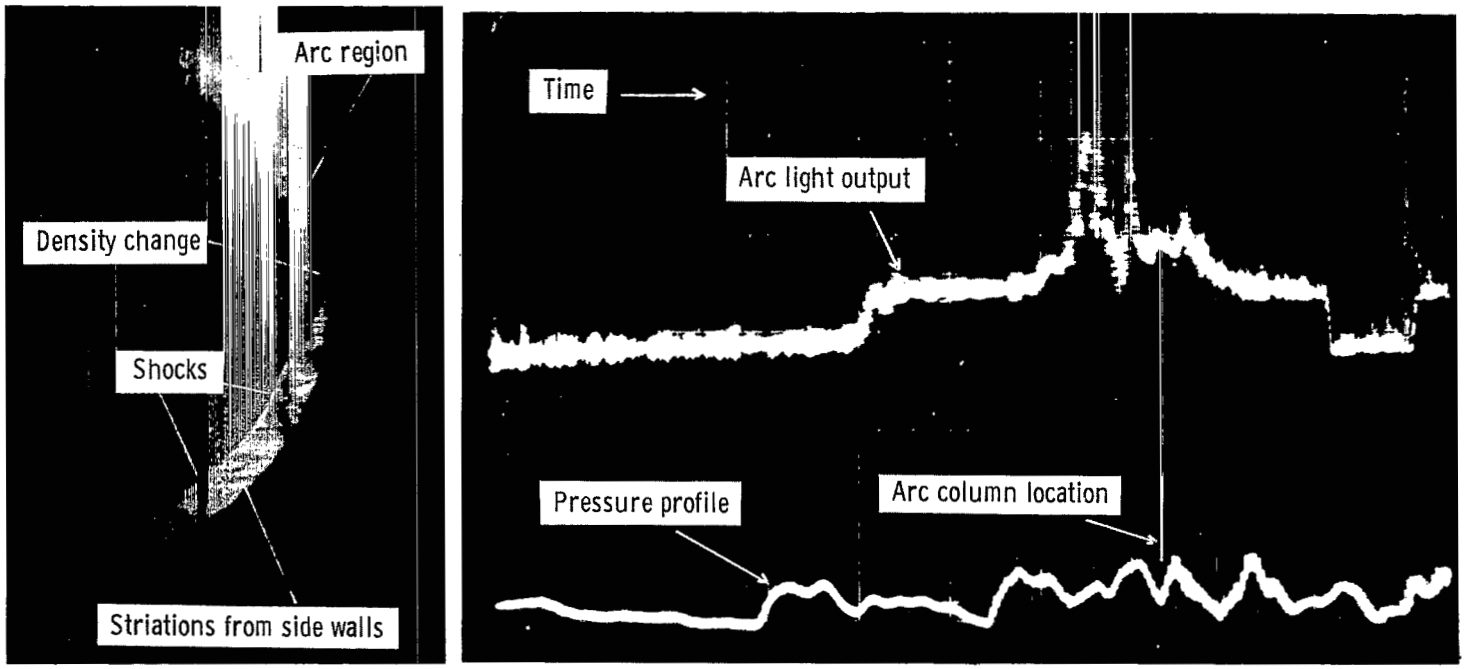

(a) Schlieren photograph.

(b) Pressure history and light output.

Figure 8.- Light output and pressure disturbance of an arc in a closed-wall circular channel at atmospheric pressure.

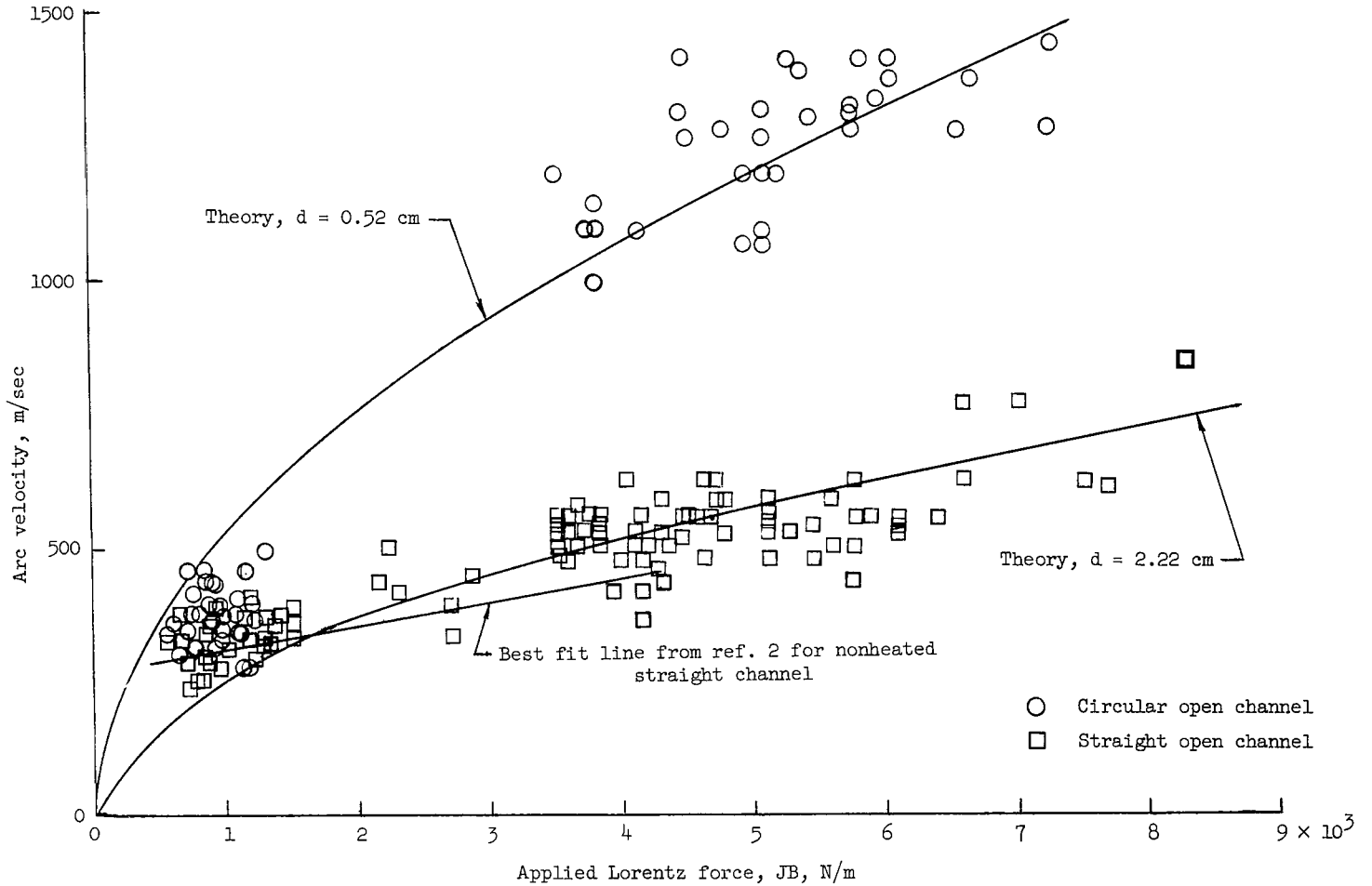

Figure 9.- Steady-state arc velocities observed in straight and circular open channels.

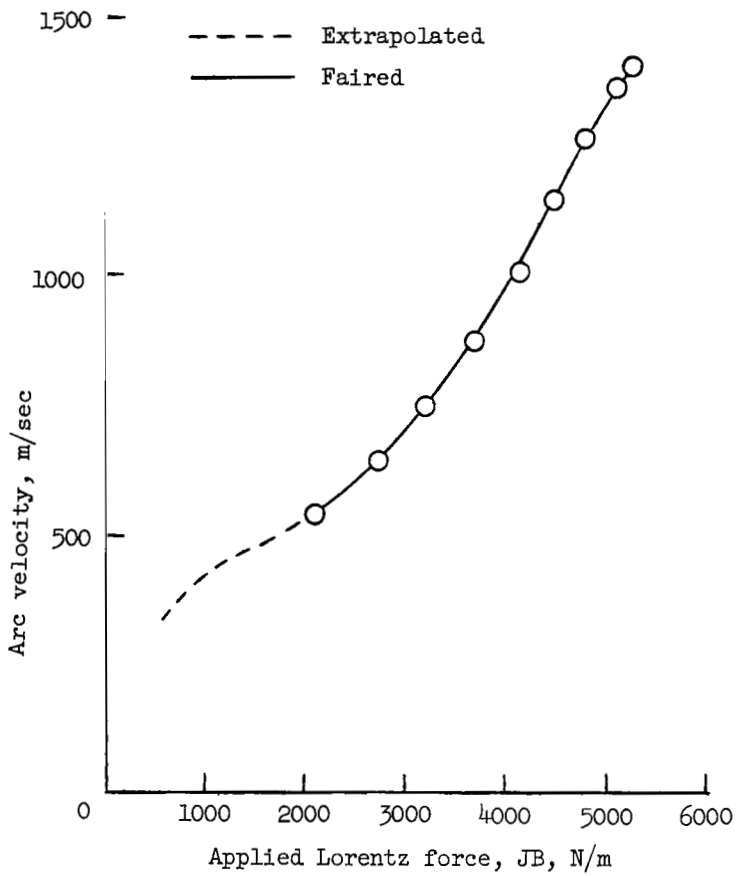

(a) Variation of velocity with applied force.

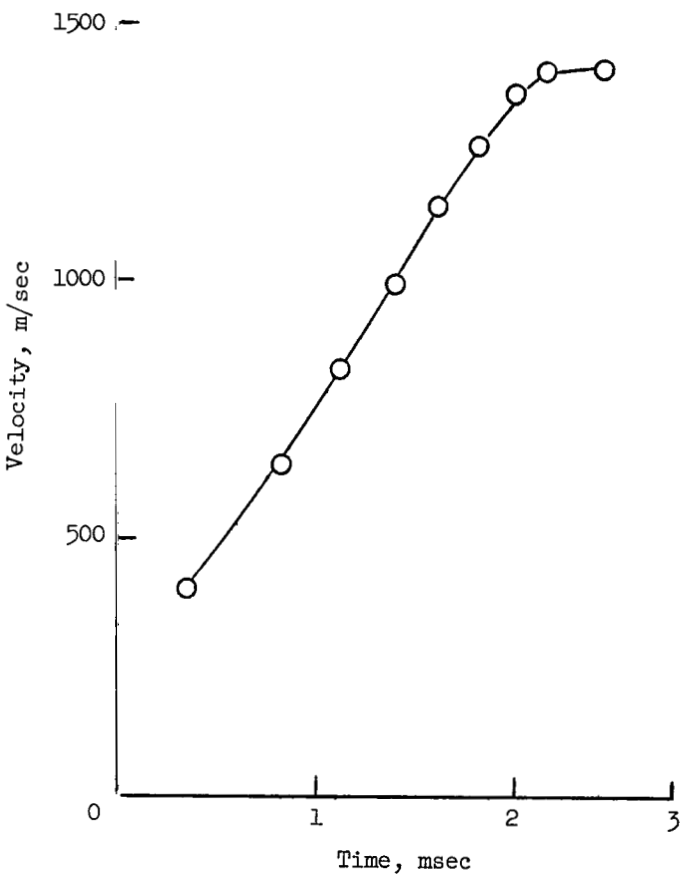

(b) Velocity time history.

Figure 10.- Velocity increase during arc start-up period.

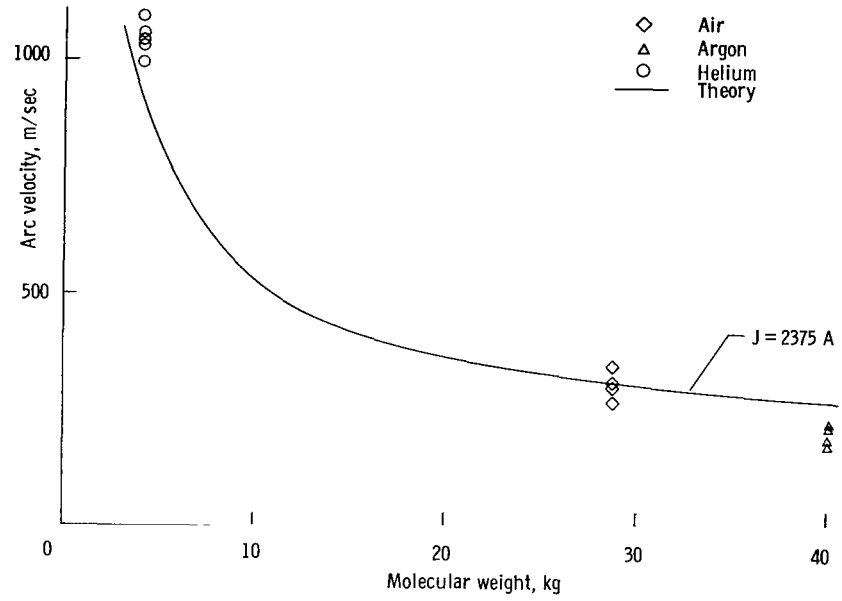

Figure 11.- Variation of the steady-state arc velocity in a circular channel with change in gas molecular weight at atmospheric pressure.

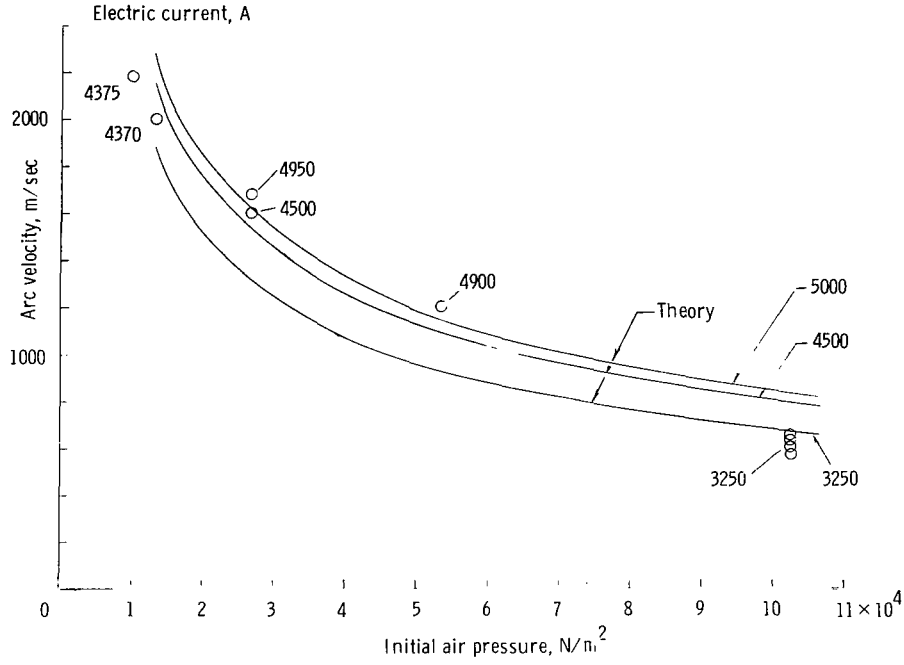

Figure 12.- Effect of initial air pressure on arc velocity in circular channel.

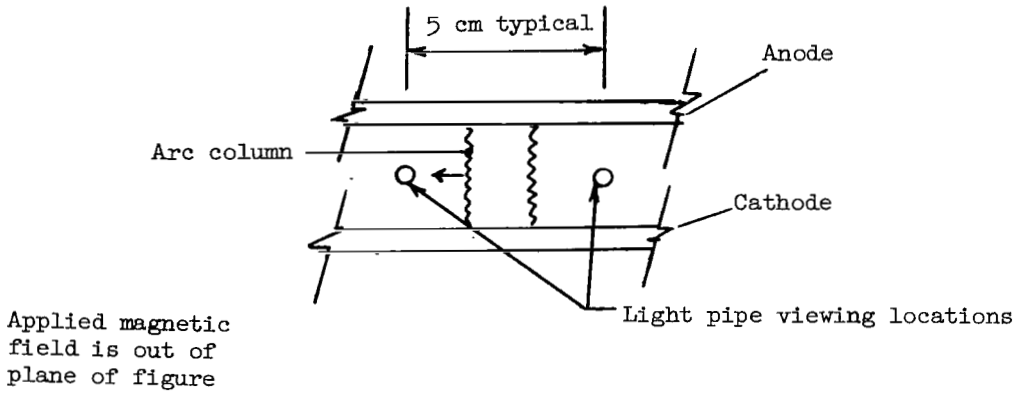

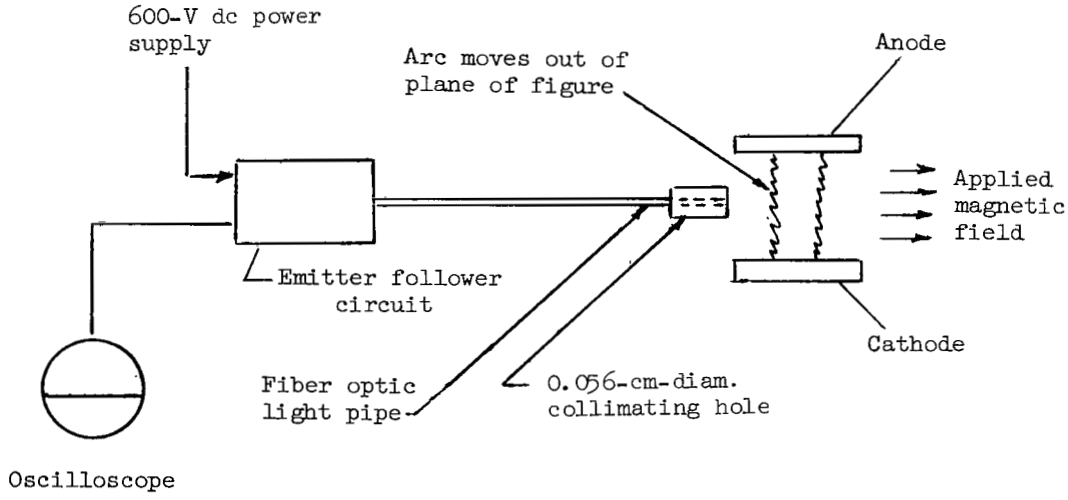

Figure 13.- Arc velocity measuring apparatus.

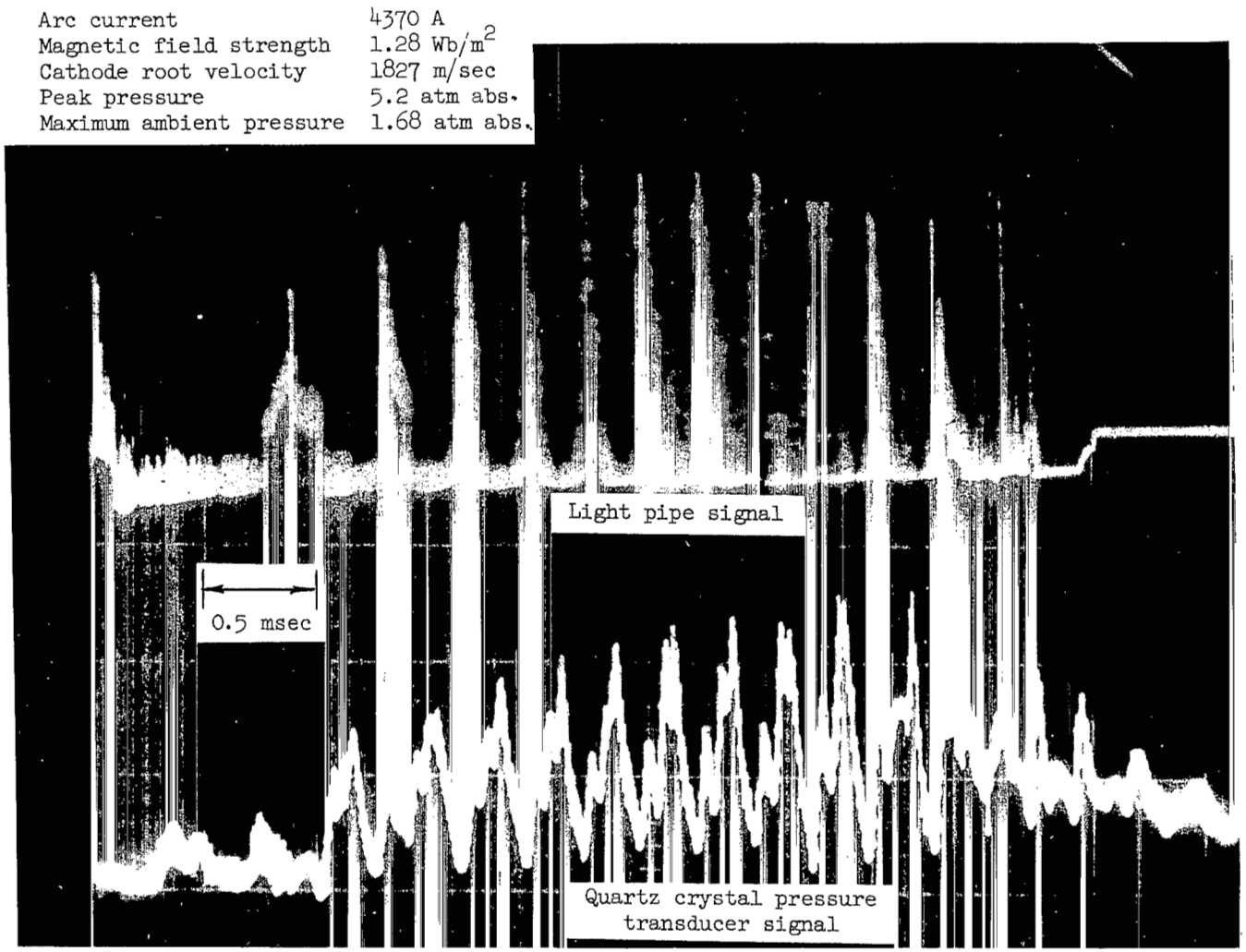

L-70-4772

Figure 14.- Circular channel light pipe and pressure signals following arc initiation. Initial pressure, 13 300 N/m^2.

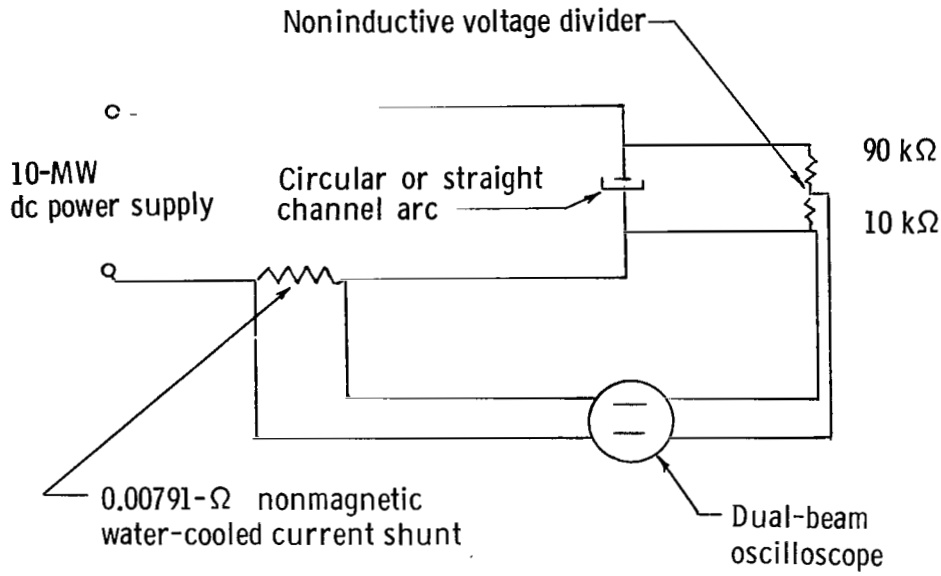

Figure 15.- Schematic of arc voltage and current measuring apparatus.

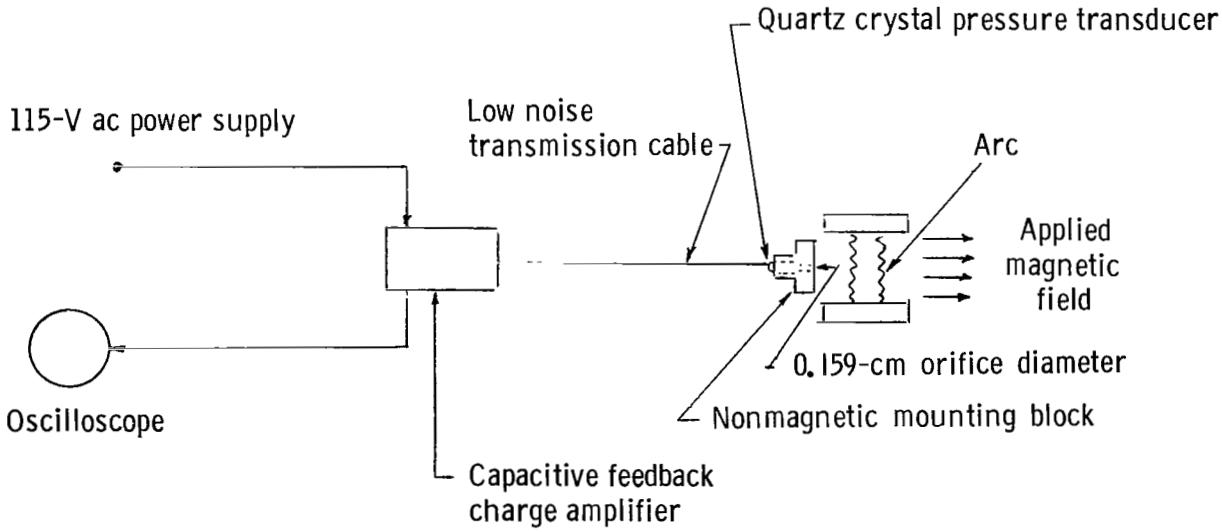

Figure 16.- Quartz crystal pressure transducer and associated apparatus.

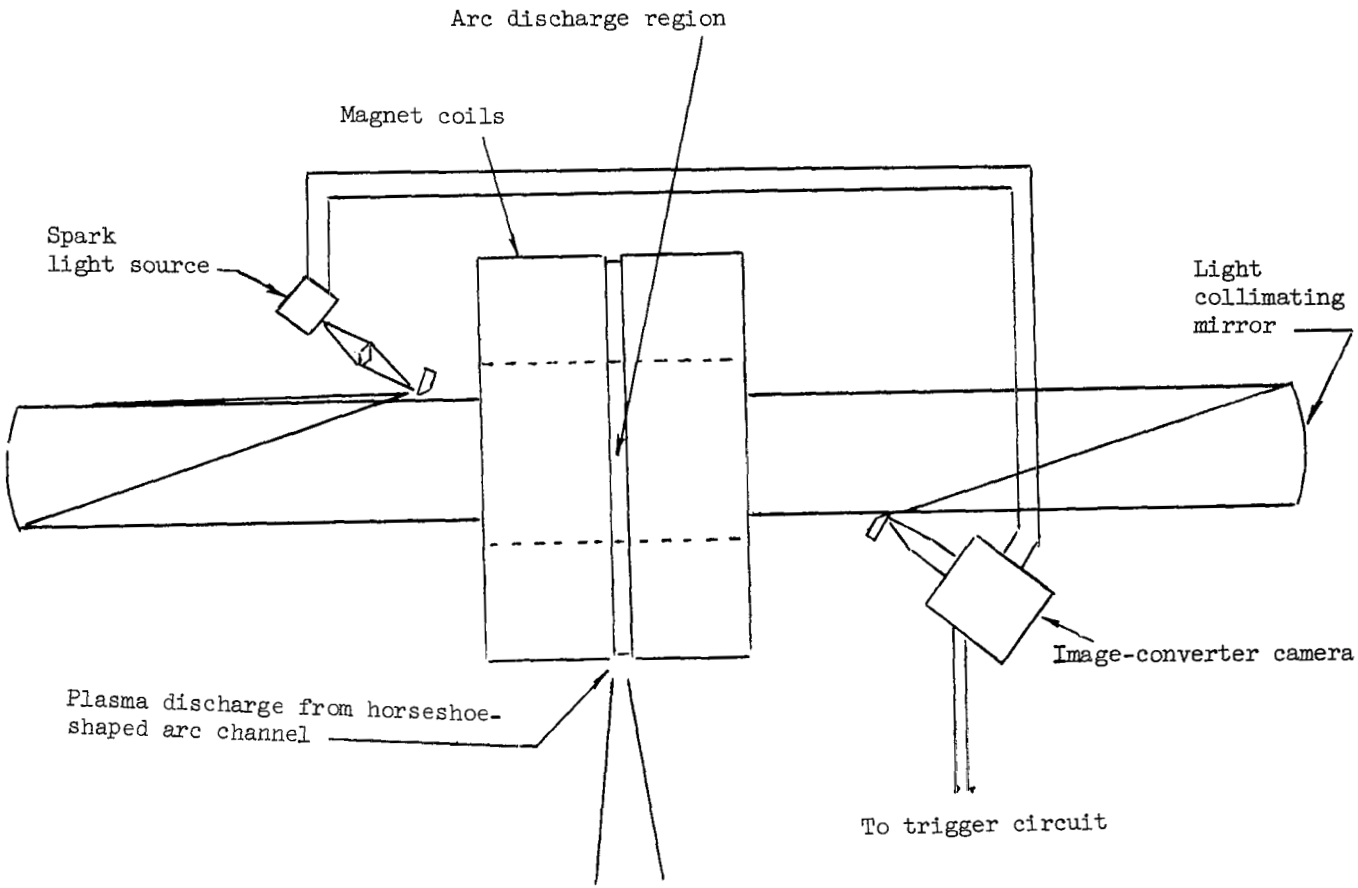

Figure 17.- Photographing system for taking either schlieren or conventional pictures of arcs.

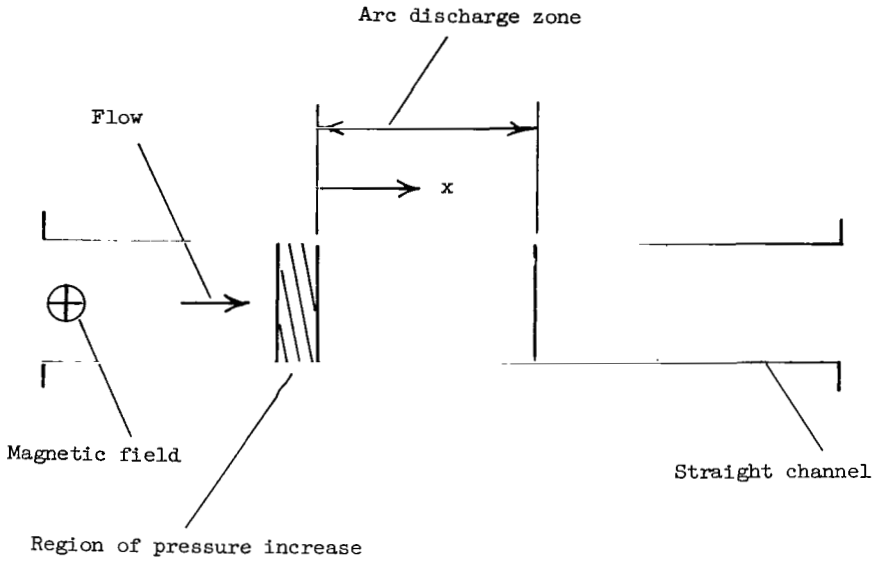

Figure 18.- Model used for theoretical study of phenomenon within a moving arc column.

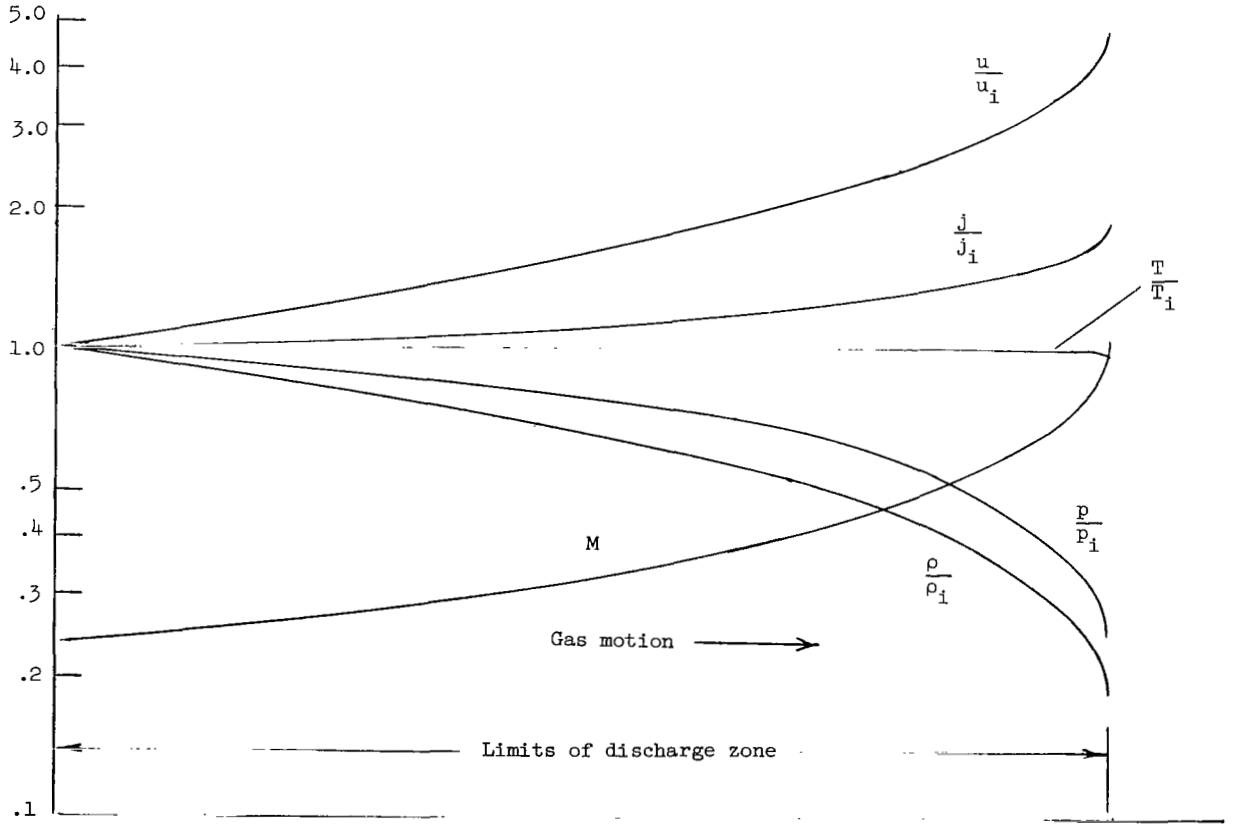

Figure 19.- Characteristic variations of calculated flow properties within the arc discharge zone.

"The aeronautical and space activities of the United States shall be conducted so as to contribute . . . to the expansion of human knowledge of phenomena in the atmosphere and space. The Administration shall provide for the widest practicable and appropriate dissemination of information concerning its activities and the results thereof."

—NATIONAL AERONAUTICS AND SPACE ACT OF 1958

NASA SCIENTIFIC AND TECHNICAL PUBLICATIONS

TECHNICAL REPORTS: Scientific and technical information considered important, complete, and a lasting contribution to existing knowledge.

TECHNICAL NOTES: Information less broad in scope but nevertheless of importance as a contribution to existing knowledge.

TECHNICAL MEMORANDUMS: Information receiving limited distribution because of preliminary data, security classification, or other reasons.

CONTRACTOR REPORTS: Scientific and technical information generated under a NASA contract or grant and considered an important contribution to existing knowledge.

TECHNICAL TRANSLATIONS: Information published in a foreign language considered to merit NASA distribution in English.

SPECIAL PUBLICATIONS: Information derived from or of value to NASA activities. Publications include conference proceedings, monographs, data compilations, handbooks, sourcebooks, and special bibliographies.

TECHNOLOGY UTILIZATION PUBLICATIONS: Information on technology used by NASA that may be of particular interest in commercial and other non-aerospace applications. Publications include Tech Briefs, Technology Utilization Reports and Notes, and Technology Surveys.

Details on the availability of these publications may be obtained from:

SCIENTIFIC AND TECHNICAL INFORMATION DIVISION

NATIONAL AERONAUTICS AND SPACE ADMINISTRATION

Washington, D.C. 20546